Dalton Transactions

PAPER

View Article Online
View Journal | View Issue

Cite this: *Dalton Trans.*, 2017, **46**, 10255

Coming full circle: constructing a [Gd_6] wheel dimer by dimer and the importance of spin topology†

Thomas N. Hooper,[a] Stuart K. Langley,‡[b] Silvia Gómez-Coca,[c] Giulia Lorusso,[d] Eliseo Ruiz,[c] Keith S. Murray,*[b] Marco Evangelisti*[d] and Euan K. Brechin*[a]

The syntheses, structures, magnetic and thermodynamic properties of three related triethanolamine-based Gd^{III} complexes are described. The smallest, a dimer ([Gd_2]), can be viewed as the subunit from which the two larger complexes, a linear tetramer ([Gd_2]$_2$) and a cyclic hexamer ([Gd_2]$_3$), are composed by further deprotonation of the triethanolamine ligand. In all cases, nearest neighbour magnetic ions are weakly correlated by antiferromagnetic isotropic exchange, whose strength does not change significantly from one complex to another; J ranging from −0.10 to −0.13 cm^{-1}. Therefore, rather than the strength of the coupling, it is the spin topology that is the dominant factor in determining the differences between the physical properties – specifically, the nuclearity and the transition from open (dimer and tetramer) to cyclic (hexamer) boundary conditions. Indeed the hexanuclear wheel reaches the continuum limit of classical Heisenberg spin chains. In terms of the magnetocaloric properties, the smaller the nuclearity, the larger the magnetic entropy and adiabatic temperature changes.

Received 23rd June 2017,
Accepted 18th July 2017

DOI: 10.1039/c7dt02281f

rsc.li/dalton

Introduction

Molecule-based materials consist of molecular building blocks that can be linked together in various ways to create larger, more complex 0–3D species. The type and magnitude of the interactions between the molecular units is crucial in determining their physical properties. If magnetic ions are involved, then molecule-based magnetic materials can provide a route for testing model spin systems.[1] In this regard, chemical synthesis is a powerful tool because it can lead to a bottom-up approach to examining magnetic interactions in a controlled fashion and, as such, to materials with designer properties.[2] Here, we focus on isotropic metal ions, namely Gd^{III}, whose quenched orbital momentum implies that crystal field effects are extremely small, if not negligible.[3] Furthermore, gadolinium possesses the largest spin (s = 7/2) of any ion in the periodic table. Under these circumstances, classical spin models can provide a good approximation to systems of interacting quantum spins.

From an applications perspective, the aforementioned characteristics contribute to making gadolinium the most widely employed element in magnetocaloric materials.[4] The magnetocaloric effect (MCE) is based on the changes of magnetic entropy (ΔS_m) and adiabatic temperature (ΔT_{ad}) upon application of a magnetic field and is of interest for refrigeration *via* a process known as adiabatic demagnetization.[5] Although the MCE is intrinsic to all magnetic materials, in only a few of these are the changes sufficiently large to make them commercially suitable. Molecular magnetic refrigerants are amongst the most promising candidates in this regard, with recent examples demonstrating an MCE comparable to materials conventionally employed for low- and ultra-low-temperature cooling applications.[6] These improvements have allowed the desired physical characteristics of the ideal molecule-based materials to be identified.[4b] These are: (1) A large spin s, since the magnetic entropy is related to it by $S_m = R \ln(2s + 1)$, where R is the gas constant. (2) Molecular isotropy, since zero-field splitting promotes spin ordering, limiting the MCE at the lowest temperatures. (3) Weak magnetic inter-

[a]*EaStCHEM School of Chemistry, The University of Edinburgh, David Brewster Road, Edinburgh, EH9 3FJ, UK. E-mail: ebrechin@ed.ac.uk*
[b]*School of Chemistry, Monash University, Clayton, Victoria 3800, Australia. E-mail: keith.murray@monash.edu*
[c]*Departament de Química Inorgànica I Orgànica and Institut de Recerca de Química Teòrica i Computacional, Universitat de Barcelona, Diagonal 645, 08028 Barcelona, Spain*
[d]*Instituto de Ciencia de Materiales de Aragón, CSIC-Universidad de Zaragoza, 50009 Zaragoza, Spain. E-mail: evange@unizar.es*

†Electronic supplementary information (ESI) available: Packing diagrams, magnetization data, magnetic entropy data, computational details. CCDC 1520393 and 1520394. For ESI and crystallographic data in CIF or other electronic format see DOI: 10.1039/c7dt02281f

‡Current address: School of Science and the Environment, Division of Chemistry, Manchester Metropolitan University, Manchester M15 6BH, UK.

actions, which lead to low-lying excited states each of which contribute to the field dependence of the MCE. (4) A (relatively) low molecular mass, and thus a large magnetic density. These four prerequisites therefore dictate the synthetic strategy towards constructing good magnetic refrigerants. A sensible approach is based on the synthesis of homo- and heterometallic Gd^{III} clusters. The inherently weak exchange mediated through the core-like f-orbitals of Gd^{III} and its isotropic f^7 configuration guarantee the presence of multiple low-lying spin states. Heterometallic complexes (*e.g.*, Gd^{III}–TM^{n+}; TM = transition metal) can be guaranteed to afford non-zero spin ground states on account of their differing d^n/f^n electron configurations and on the basis of literature precedents that show certain combinations, *e.g.*, Gd^{III}–Cu^{II}, favour ferromagnetic exchange.[7] Molecular isotropy can be controlled through the use of isotropic metals ions (Gd^{III}, Cr^{III}, Mn^{II}, Fe^{III}), or *via* the synthesis of highly symmetric molecules. The latter usually result from high temperature/high pressure reactions, *i.e.*, they are the thermodynamic products of solvothermal or microwave synthesis, and this then allows the use of anisotropic metal ions.[8]

We, and others, have demonstrated that, upon deprotonation, triethanolamine (H_3tea) is an excellent ligand for constructing high spin, high nuclearity compounds,[9] including a $[Cu_5Gd_4]$ cluster displaying a large cryogenic MCE.[10] Herein we extend the coordination chemistry of triethanolamine to homometallic Gd^{III} species and show that stepwise structural variation can be provided by progressive deprotonation of the ligand, and that the initial compound made, a dimer, can be regarded as the building block from which a tetramer and hexamer can be constructed. The structure of the hexamer has been previously communicated.[9f] We construct the magnetic and thermodynamic properties of these compounds in the same manner, since the exchange interaction that characterizes the dimeric subunit remains effectively unchanged in the tetramer and hexamer.

Results and discussion

The reaction of $Gd(NO_3)_3{\cdot}6H_2O$ with H_3tea in the presence of 1 equivalent of base (acetate) in methanol results in the formation of the alkoxide bridged gadolinium dimer $[Gd(H_2tea)(NO_3)_2]_2{\cdot}2MeOH$ (**1**·2MeOH, Fig. 1; see the Experimental section for full details). This is the basic building block common to all the clusters reported herein. Crystals suitable for X-ray diffraction were grown from diffusion of diethyl ether into the alcoholic reaction mixture.

The Gd^{III} ions are bridged by two μ-O-atoms (O1 and symmetry equivalent (s.e.)) derived from the sole deprotonated arm of two triethanolamine ligands to form a planar $[Gd_2O_2]^{4+}$ motif. Each Gd^{III} ion is 9-coordinate in capped square-antiprismatic geometry with a $[GdO_8N]$ coordination sphere. The eight remaining coordination sites are filled by a combination of two chelating nitrate ions, two terminally bonded O-atoms (O2, O3) from the protonated arms of the H_2tea ligand, and

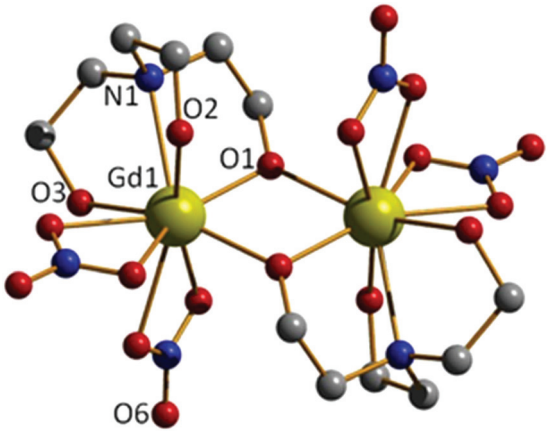

Fig. 1 The molecular structure of **1**. Colour code: Gd, yellow; O, red; N, blue; C, grey. H-atoms and MeOH solvate molecules have been omitted for clarity. Gd–O(NO_3), 2.495–2.577 Å; Gd–O(H_2tea), 2.301–2.491 Å; Gd–N(H_2tea), 2.679 Å.

the N-atom (N1) from the H_2tea ligand. The bond lengths in the $[Gd_2O_2]$ core show slight asymmetry {Gd(1)–O(1) 2.301(4) Å and Gd(1)–O(1A) 2.250(4) Å} and the Gd(1)–O(1)–Gd(1A) bond angle of 109.11(16)° means the Gd···Gd distance of 3.706(7) Å is one the shortest reported for a planar $[Gd_2O_2]$ motif. This small Gd···Gd distance is consistent with known alkoxide-bridged Gd^{III} dimers,[11–15] with carboxylate bridged dimers tending to show larger Gd···Gd separations, as would be expected from the presence of a three atom O–C–O bridge.[16]

In the crystal molecules of **1** pack in chains in the *bc* plane as directed by H-bonding interactions between the alcohols from the triethanolamine ligands to both the non-coordinated O-atoms of the nitrate anions {O(3)···(O6) 2.762 Å} and the MeOH solvate molecules {O(2)···(O10) 2.644 Å, O(3)···(O10) 2.953 Å} that sit between neighbouring clusters (Fig. S1†).

A similar reaction between $Gd(NO_3)_3{\cdot}6H_2O$ and H_3tea in MeOH with 1 equivalent of acetate and 1.5 equivalents of NEt_3 yields the tetrametallic cluster $[Gd_2(H_2tea)(Htea)(NO_3)_3]_2{\cdot}MeOH$ (**2**·MeOH; Fig. 2). Complex **2** can be regarded as the linear dimer of complex **1**. Single crystals of **2** suitable for X-ray

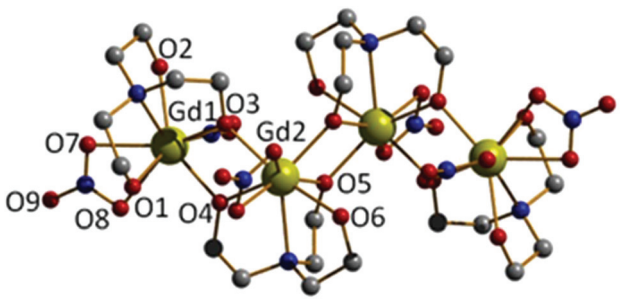

Fig. 2 The molecular structure of **2**. Colour code: Gd, yellow; O, red; N, blue; C, grey. H-atoms and MeOH solvate molecules have been omitted for clarity. Gd–O(NO_3), 2.480–2.569 Å; Gd–O(H_2tea/Htea), 2.264–2.468 Å; Gd–N(H_2tea/Htea), 2.611–2.646 Å.

diffraction were formed from diffusion of diethyl ether into the methanolic reaction mixture. The structure describes a zig-zag like chain structure in which two molecules of **1** have dimerised in a head-to-tail fashion *via* the "further" deprotonation of two of the triethanolamine ligands (*i.e.*, H_2tea to Htea). The doubly deprotonated $Htea^{2-}$ ligands chelate to the central Gd^{III} ions (Gd2 and s.e.), using one alkoxide arm each to bridge between Gd2–Gd2A (O5 and s.e.), and the other (O4 and s.e.) to bridge to the peripheral Gd^{III} ions (Gd1 and s.e.). The singly deprotonated H_2tea^- ligands chelate to Gd1 (and s.e.), with the protonated arms terminally bonded, and the sole deprotonated arm (O3 and s.e.) μ–bridging to Gd2 (and s.e.). The remaining two coordination sites on each Gd^{III} ion are completed by the presence of one chelating NO_3^- anion, resulting in each of the Gd^{III} ions being in a capped square-antiprismatic geometry with a $[GdO_8N]$ coordination sphere. This arrangement is reinforced by an intra-molecular H-bond between the OH of the triethanolamine attached to the central Gd^{III} centre (Gd2) and the coordinated oxygen of a nitrate anion attached to the terminal Gd^{III} centre {O(6)···(O11) 2.736 Å}. The bond lengths and angles found in **2** are similar to those in **1** with asymmetry observed in the planar $[Gd_2O_2]$ bridge and short Gd···Gd distances.

There are numerous inter-molecular interactions in the crystal, with each molecule of **2** being H-bonded to its four nearest neighbours, two above and two below opposite ends of the Gd_4 plane. As in **1** these are directed by one NO_3^-···HO(triethanolamine) {O(8)···(O2) 2.760 Å} interaction, and by O(NO_3^-)···O(MeOH solvate)···OH(triethanolamine) contacts {O(12)···(O16A) 2.990 Å, O(16A)···(O1) 2.626 Å}. The result is the formation of H-bonded 2-D sheets running across the diagonal of the *ac* plane (Fig. S2†). The $[Gd_4]$ zig-zag chain structure in **2** is somewhat similar to that observed in the complex $[Dy_4L_4(MeOH)_6]$ (H_3L = 2-hydroxy-3-methoxybenzoic acid [(2-hydroxy-3-methoxyphenyl)methylene] hydrazide).[17,18]

Repeating the reaction that produced **2**, but increasing the molar ratio of NEt_3 to 2 equivalents (per mole of Gd), produces the cluster $[Gd(Htea)(NO_3)]_6{\cdot}8MeOH$ (**3**·8MeOH; Fig. 3) Complex **3** (which some of us have reported previously[9f]) can be regarded as the cyclic trimer of complex **1**. Single crystals of **3** suitable for X-ray diffraction were formed from the slow evaporation of a MeOH/CH_2Cl_2 solution. The structure is that of a hexametallic wheel in which three molecules of **1** have oligomerised in a head-to-tail fashion *via* the double deprotonation of all of the triethanolamine ligands. Each $Htea^{2-}$ ligand thus chelates to one Gd^{III} ion and bridges to two others, forming a $[Gd_6O_{12}]^{6+}$ magnetic core. As for complex **2**, each Gd^{III} ion sits in a capped square antiprismatic geometry with a $[GdO_8N]$ coordination sphere, the remaining sites per metal being occupied by one chelating NO_3^- ion. The planar asymmetric $[Gd_2O_2]$ motif is again present with the Gd···Gd distance being 3.775 Å, and the Gd···Gd distance across the diameter of the wheel measuring 7.549 Å. Each of the six $Htea^{2-}$ ligands is H-bonded to a MeOH solvate molecule (*e.g.* O3···O6, 2.682 Å) which in turn is H-bonded to either another MeOH solvate molecule or a neighbouring $[Gd_6]$ wheel {O(MeOH)···O(Htea), 2.682 Å}. The result of these inter-molecular interactions is the formation of aesthetically pleasing 2D honeycomb-like sheets in the *ab* plane (Fig. S3†). The closest inter-molecular interactions between sheets (down the *c*-axis) are between O-atoms from the NO_3^- ions and C-atoms from the $Htea^{2-}$ ligands {O···C, ~3.7 Å}.

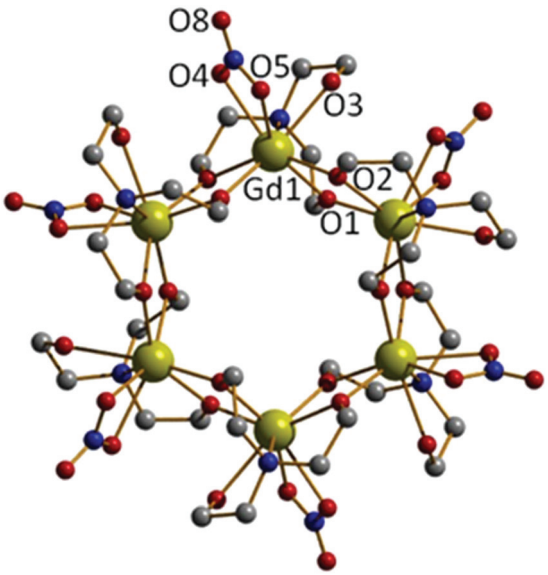

Fig. 3 The molecular structure of **3**. Colour code: Gd, yellow; O, red, N, blue, C, grey. H-atoms and MeOH solvate molecules have been omitted for clarity. Gd–O(NO_3), 2.530–2.550 Å; Gd–O(Htea), 2.269–2.339 Å; Gd–N(Htea), 2.600 Å.

The idea that complexes **1** and **2** are simply 'kinetic' products reached on the road to the 'thermodynamic' end-product **3** is strengthened by the observation that **3** can also be synthesised by simple addition of 1 equivalent of triethylamine to **1** in a mixture of methanol and dichloromethane, and that **3** can be made (in higher yield) *via* the solvothermal reaction of $Gd(NO_3)_3{\cdot}6H_2O$ and H_3tea in the complete absence of base. The relatively poor yield of **2** has prevented us from 'completing the cycle', and no attempt has yet been made to reverse the oligomerisation ($Gd_6 \rightarrow Gd_4 \rightarrow Gd_2$) *via* addition of, for example, acid. The reaction pathways are summarised in Scheme 1.

Magnetometry

DC magnetic susceptibility measurements were carried out on powdered crystalline samples of **1–3** in the 300–5 K temperature range in an applied magnetic field of 0.1 T. Plots of the $\chi_m T$ *vs.* T response are given in Fig. 4. All three complexes show similar behaviour, as one might expect given their structural similarity. Their room-temperature $\chi_m T$ values are consistent with the presence of 2 (15.5 $cm^3\ mol^{-1}$ K, **1**), 4 (32.1 $cm^3\ mol^{-1}$ K, **2**) and 6 (48.7 $cm^3\ mol^{-1}$ K, **3**) non-interacting $s = 7/2$ centres. These values remain constant as the temperature is lowered down to approximately 50 K when a sharp decrease is seen in each case, resulting in minimum values of ~10, 18 and 27 cm^3 K mol^{-1}, respectively. This is clearly

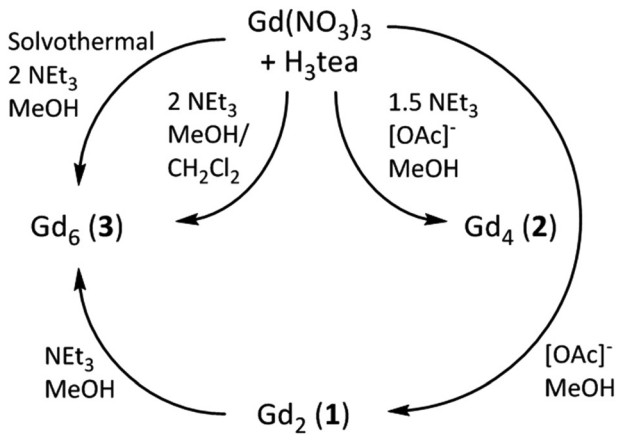

Scheme 1 Reaction pathways summarising the formation of complexes **1–3**.

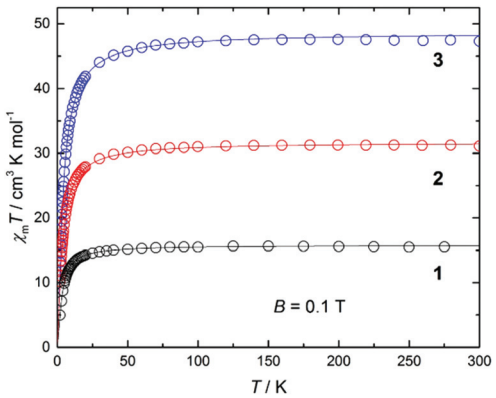

Fig. 4 Plot of $\chi_m T$ *vs.* T for complexes **1** (bottom), **2** (middle) and **3** (top) measured at 0.1 T and in the 5–300 K temperature range. The solid lines are a fit of the experimental data employing the Hamiltonians of eqn (1)–(3). See text for details.

indicative of rather weak antiferromagnetic nearest neighbour exchange interactions, consistent with previously published examples of alkoxide-bridged Gd^{III} ions.[11–15] Isothermal DC magnetization curves were also measured for powdered crystalline samples of **1–3** up to an applied magnetic field of 5 T and for several temperatures between 2 and 10 K (Fig. S4†).

The experimental susceptibility and magnetization data in each case (**1–3**) were fitted using the isotropic Hamiltonians given in Scheme 2 and eqn (1)–(3), respectively.[19] Note that we identify two different coupling constants J and J' for complex **2**, on account of the slightly different coordination environments of the Gd^{III} ions involved: the Gd(1)···Gd(2) distance is 3.735 Å, while the Gd(2)···Gd(3) distance is 3.785 Å; the Gd(1)–O–Gd(2) bond angles are 107.9° and 109.8°, while the Gd(2)–O–Gd(3) bond angles are both 110.2°. This affords, $g = 2.00$ $J = -0.13$ cm^{-1} for **1**; $g = 2.01$ $J = -0.12$ cm^{-1}, $J' = -0.10$ cm^{-1} for **2**; and $g = 2.02$ $J = -0.10$ cm^{-1} for **3** (see solid lines in Fig. 4 and S4† for the susceptibility and magnetization data, respectively). These values are comparable with another

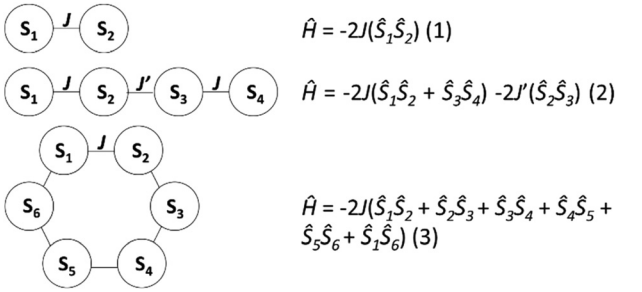

Scheme 2 The exchange interaction schemes employed to fit the susceptibility data for (top to bottom) **1–3**.

alkoxide bridged Gd^{III} dimer $[Gd(Hsabhea)(NO_3)]_2$ (where H_3sabhea = *N*-salicylidene-2-(bis-(2-hydroxyethyl)amino)ethylamine)[11] which displayed antiferromagnetic coupling of $J = -0.198$ cm^{-1} ($g = 1.975$); but is larger in absolute magnitude than that observed in carboxylate bridged dimers.[16] Note that the three complexes have very similar values of the exchange coupling constant. Thus, the magnetic properties are determined chiefly by the different spin topologies.

Electronic structure calculations

To investigate the magnetic properties of **1–3** in a little more detail, electronic structure calculations based on density functional theory (DFT) have been performed. Two different computational approaches were employed: the SIESTA code[20] with the PBE functional,[21] and FHI-Aims[22] with implemented hybrid B3LYP[23] functional which also allows us to include relativistic effects using the ZORA approach (see Computational details in the ESI†). Both methodologies have been successfully employed to calculate exchange coupling constants.[24] The DFT calculated J values are collected in Table 1. Both computational approaches correctly reproduce the weak antiferromagnetic exchange interactions typically observed for Gd^{III} ions bridged by alkoxide ligands. Taking into account the very weak nature of these interactions, they reproduce the observed coupling constants remarkably well, although the SIESTA code with PBE functional tends to overestimate the J values somewhat.[24] Interestingly, the inclusion of scalar relativistic effects together with a hybrid functional is necessary to obtain J values close to the experimental values.

For the sake of completeness, we have also studied the dependence of the exchange coupling constant on the bridging Gd–O–Gd angle. Calculations were performed on a model

Table 1 Experimental and calculated magnetic exchange interactions (in cm^{-1}) for complexes **1**, **2** and **3** (see main text and ESI for details)

		J_{exp}	J_{PBE}	J_{B3LYP}	$J_{B3LYP+ZORA}$
1	J	−0.13	−0.22	−0.20	−0.16
2	J	−0.12	−0.24	−0.18	−0.15
	J'	−0.10	−0.17	−0.14	−0.13
3	J	−0.10	−0.20	−0.15	−0.13

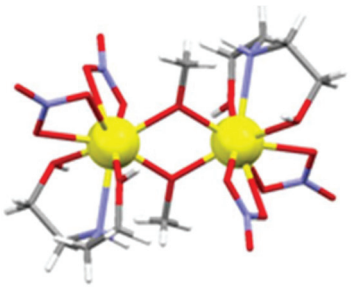

Fig. 5 The model complex employed to calculate the exchange interactions between Gd^{III} ions upon changing Gd–O–Gd angle. Colour code: Gd, yellow; O, red; N, blue; C, grey; H, white.

complex (Fig. 5) derived from **1** in which the 'second' $-CH_2-$ moiety of the triethanolamine arm linking the bridging O-atom to the N-atom has been replaced with two H-atoms, thus forming independent bridging (methoxide) and terminal ligands. The results, for a symmetric model with Gd–O bond distances fixed at 2.3 Å, are summarized in Fig. 6. They show that the strength of the antiferromagnetic coupling increases on lowering the Gd–O–Gd angle, and that this coupling is weakly antiferromagnetic in the range of bridging angle values employed.

Heat capacity

Heat capacity experiments were carried out in the 0.3–30 K temperature range in applied magnetic fields of 0, 1, 3 and 7 T. Plots of the c_p *vs.* T response are given in Fig. 7. Above *ca.* 6 K, c_p is dominated by lattice phonon modes of the crystal, which can be described by the Debye model (dotted line) and simplify to $c_p/T^3 = 1.1 \times 10^{-3}$, 3.3×10^{-3} and 3.0×10^{-3} K^{-3} at the lowest temperatures for **1**, **2** and **3**, respectively.

The magnetic field-dependent contribution to the heat capacity (c_m) develops at the lowest temperatures and shows characteristics that are common to all three complexes. For each complex, the c_m curves collected for $B = 0$ and 1 T are essentially indistinguishable from one another. This behaviour is consistent with dominant antiferromagnetism, in agreement

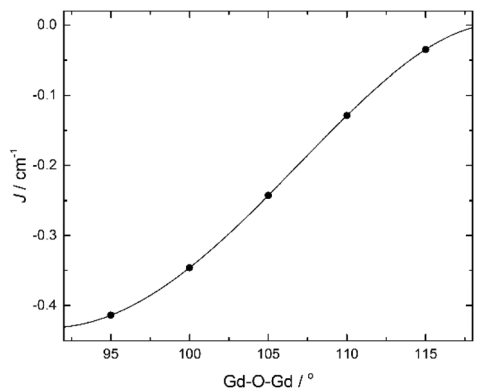

Fig. 6 Calculated B3LYP J-values *vs.* Gd–O–Gd angle for a symmetric $[Gd^{III}_2]$ model (Fig. 5) with Gd–O bond distances fixed at 2.3 Å.

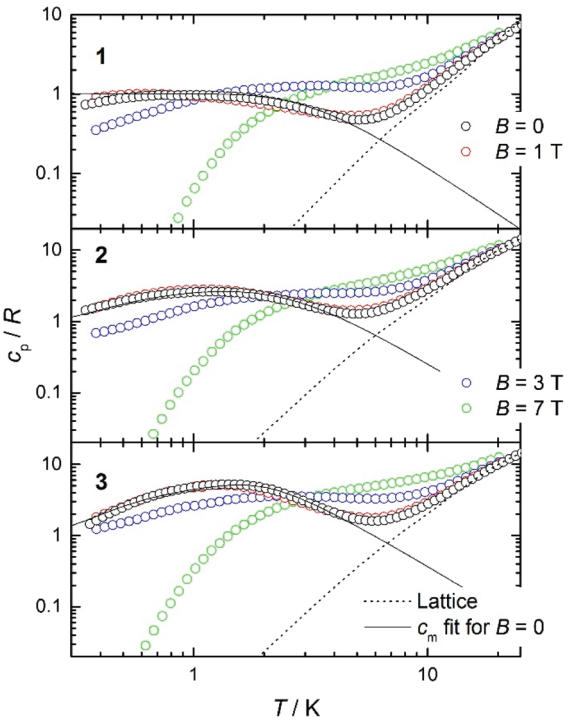

Fig. 7 Plots of the molar heat capacity, normalized to the gas constant, c_p/R *vs.* T for complexes **1** (top), **2** (middle) and **3** (bottom) measured at the indicated applied magnetic field values and in the 0.3–30 K temperature range. The solid line is the calculated zero-field magnetic contribution c_m, while the dotted line is the lattice contribution. See text for details.

with the magnetization data. For the highest field used ($B = 7$ T), all spins are fully decoupled and the magnetic anomaly is therefore equivalent to a Schottky curve originating from the field-splitting of non-interacting Gd^{III} spins. Comparing the three complexes, the only difference between the c_m curves for $B = 7$ T is the height of the anomaly, which is proportional to the number of spins per mole involved. In addition to the height, what differs in the magnetic heat capacity from one compound to another is the temperature at which the zero-field c_m has its maximum – this temperature is clearly higher in **3** than in **2** and **1**, respectively (see Fig. 7). Note that intermolecular (dipolar) interactions play a negligible role, at least at the relatively high temperatures investigated. The experimental zero-field c_m curves are indeed satisfactorily modelled (solid lines) by the isotropic Hamiltonians given in Scheme 2 and eqn (1)–(3), using the same parameters obtained from the fits of the magnetization data.

Spin topology

In order to highlight the role of the spin topology and to facilitate comparison between the physical properties of **1**, **2** and **3**, we normalize the susceptibility and heat capacity data per Gd^{III} ion and plot the $\chi_m^{(Gd)}$ and $c_m^{(Gd)}$ in Fig. 8. Furthermore, we normalize χ_m and T per $|J|$, whose values were obtained from the fits of the experimental data to the Hamiltonians of eqn

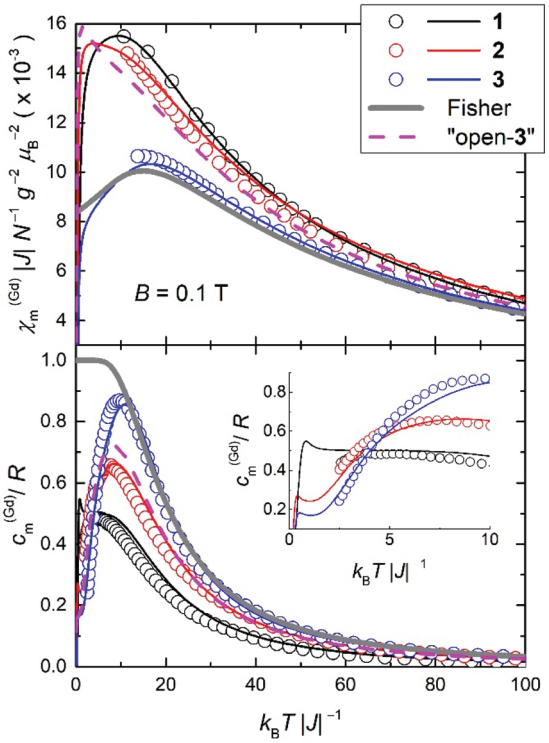

Fig. 8 Plots of experimental molar χ_m for B = 0.1 T (top) and zero-field c_m (bottom), normalized per Gd^{III} ion, *vs.* T for complexes **1**, **2** and **3**, as labelled. Temperatures and χ_m are further normalized per the exchange constant $|J|$. Thin solid lines are calculated employing the Hamiltonians of eqn (1)–(3). The thick solid line is Fisher's model for isotropic Heisenberg chains in the limit of infinite spins. The dashed line is calculated for "open-**3**", *i.e.*, an analogue of **3** with imposed open boundary conditions. See text for details. Inset: Magnification of the low-temperature heat capacity.

(1)–(3). For **2**, we assume $|J|$ = 0.11 cm^{-1}, as a mean value between 0.10 and 0.12 cm^{-1} (see fit). Note that since all the J values involved are very close to one another, normalization of the temperature is not strictly necessary for comparison. Importantly, Fig. 8 reveals strikingly different behaviours depending on the spin topology. Complex **1** has a larger $\chi_m^{(Gd)}$ with respect to **2** and **3**, while the opposite trend applies to the $c_m^{(Gd)}$ data. For comparison, we also plot the susceptibility and heat capacity calculated on basis of Fisher's model for isotropic Heisenberg infinite chains in the classical limit of infinite spins.[25] Bear in mind that the so-obtained heat capacity is unrealistic for the lowest temperatures since in the classical limit the calculation necessarily flattens and goes to a nonzero value for $T \rightarrow 0$. As can be seen in Fig. 8, both $\chi_m^{(Gd)}$ and $c_m^{(Gd)}$ of **1**, **2** and **3** gradually approach the classical limit on increasing the number of spin sites. It indeed turns out that complex **3** can be described well by Fisher's model, at least down to $k_B T|J|^{-1} \sim 10$, *i.e.*, $T \sim 1$ K. This comparison suggests that s = 7/2 spins can be regarded as classical 'infinite' spins and that the Heisenberg 1D chain of classical spins can be efficiently mapped onto a molecular wheel motif based on six Gd^{III} spins, as for **3**. Finally, to investigate the role of boundary conditions, we have considered a hypothetical molecular analogue of **3** but with an open-wheel structure, *viz.*, we break the cyclic boundary condition by omitting a J-pair in our calculations for **3**. We have calculated the susceptibility and heat capacity of "open-**3**" (dashed lines in Fig. 8), which are rather different from Fisher's model, and relatively close to the corresponding contributions for **2**. We conclude therefore that boundary conditions play a determinant role in the magnetic and thermodynamic properties of these compounds.

For $k_B T|J|^{-1} \leq 3$, thus beyond the temperature window of our experiments, the calculations show that the fewer the spin sites, the higher is the corresponding $c_m^{(Gd)}$ (inset of Fig. 8), which corresponds to an entropy (S) content higher in **1** than **2** and **3**, respectively, at the lowest temperatures. The temperature and field dependence of the entropy can be obtained by applying $S(T,B) = \int [c_p(T',B)/T']dT'$ to the heat capacity.

Magnetocalorics

We employ the experimental magnetization and heat capacity data (Fig. S4† and Fig. 7, respectively) to calculate the magnetocaloric effect for **1**, **2** and **3**, using standard procedures.[4a,b] Fig. S5† shows the magnetic entropy change, as derived by applying the Maxwell equation to the magnetization data. Likewise, Fig. 9 shows $-\Delta S_m(T, \Delta B)$ data for applied-field changes ΔB = (3–0) and (7–0) T, as derived from the entropy curves (Fig. S6†). Both calculations of the $-\Delta S_m(T, \Delta B)$ sets of data provide identical results, that we plot separately (Fig. 9 and Fig. S5†) for the sake of clarity, validating the procedures

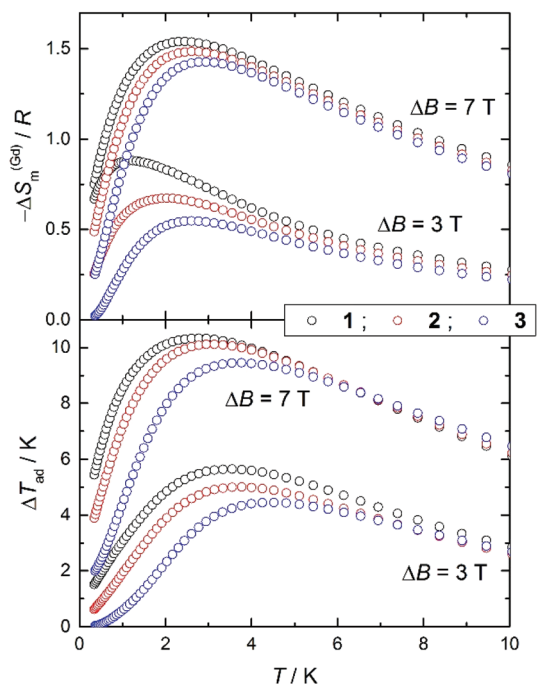

Fig. 9 For complexes **1**, **2** and **3**, plots of the magnetic entropy change, normalized per molar Gd (top) and adiabatic temperature change (bottom) *vs.* T for applied-field changes ΔB = (3–0) and (7–0) T, as derived from the corresponding heat capacity data.

employed. To facilitate the comparison between **1**, **2** and **3**, we normalize the magnetic entropy change data per molar Gd content. Similarly, we employ the entropy curves in Fig. S6† to derive the adiabatic temperature changes plotted in Fig. 9. We restrict our analysis to the ΔB = (3–0) and (7–0) T applied changes, thus omitting the data collected for 1 T since these are indistinguishable from the equivalent sets of zero-field data.

For ΔB = 7 T, Fig. 9 shows that complex **1** attains the maximum $-\Delta S_m^{(Gd)} = 1.54R$, equivalent to 27.8 J kg^{-1} K^{-1} per unit mass, at T = 2.3 K and ΔT_{ad} = 10.3 K at T = 2.8 K; complex **2** attains $-\Delta S_m^{(Gd)} = 1.48R$ = 29.8 J kg^{-1} K^{-1} at T = 2.6 K and ΔT_{ad} = 10.1 K at T = 3.1 K; complex **3** attains $-\Delta S_m^{(Gd)} = 1.43R$ = 29.0 J kg^{-1} K^{-1} at T = 2.9 K and ΔT_{ad} = 9.4 K at T = 3.8 K. Finally, for ΔB = 3 T, complex **1** attains $-\Delta S_m^{(Gd)} = 0.88R$ = 15.9 J kg^{-1} K^{-1} at T = 1.2 K and ΔT_{ad} = 5.6 K at T = 3.5 K; complex **2** attains $-\Delta S_m^{(Gd)} = 0.67R$ = 13.5 J kg^{-1} K^{-1} at T = 1.9 K and ΔT_{ad} = 5.0 K at T = 3.6 K; complex **3** attains $-\Delta S_m^{(Gd)} = 0.55R$ = 11.1 J kg^{-1} K^{-1} at T = 2.6 K and ΔT_{ad} = 4.4 K at T = 4.5 K. Although these values are relatively large for magnetic molecules based purely on Gd^{III} ions,[4c] they are much smaller than, for example, that reported for the ferromagnetic molecular dimer gadolinium acetate tetrahydrate.[26] It is interesting to compare the different behaviours in connection with the number of Gd^{III} spin centres involved, while holding 'constant' the exchange coupling. Clearly, one can notice the relatively lower MCE for complex **3**, or by analogy, for an infinite chain of classical spins. The effect can be made larger by localizing the exchange interactions into smaller spin segments, such as in **2** and **1**. This behaviour is entirely determined by the zero-field c_m and hence by the zero-field magnetic entropy. As already observed, the zero-field magnetic entropy develops closer to absolute zero for the smaller molecules.

Conclusions

We have shown that three related gadolinium complexes can be synthesised using triethanolamine as a supporting ligand, with the structural variation provided by the extent of deprotonation of the ligand. The simplest of these, a dimer (**1**), can be viewed as the building block from which the tetramer (**2**) and the hexamer (**3**) were formed in solution by further deprotonation of the triethanolamine. Complex **3** can also be synthesised by simple addition of 1 equivalent of triethylamine to **1** in a mixture of methanol and dichloromethane, and (in higher yield) *via* the solvothermal reaction of $Gd(NO_3)_3{\cdot}6H_2O$ and H_3tea in the complete absence of base. The complexes show short Gd···Gd distances and a magnetic core comprising planar $[Gd_2O_2]$ moieties. Each exhibits weak antiferromagnetic nearest neighbour exchange. Topological size effects are responsible for the magnetic and thermodynamic properties of these compounds. By decreasing the nuclearity, the magnetocaloric effect becomes larger at relatively lower temperatures, being more prominent for the dimer that reaches $-\Delta S_m$ = 27.8 J kg^{-1} K^{-1} at T = 2.3 K and ΔT_{ad} = 10.3 K at T = 2.8 K.

Experimental

$[Gd(H_2tea)(NO_3)_2]_2{\cdot}2MeOH$ (1·2MeOH)

Triethanolamine (0.5 cm^3, 1.0 M solution in MeOH, 0.5 mmol) was added to a solution of $Gd(NO_3)_3{\cdot}6H_2O$ (0.226 g, 0.5 mmol) in MeOH (25 cm^3). $[NEt_4][OAc]{\cdot}4H_2O$ (0.131 g, 0.5 mmol) was added and the solution stirred for 1 h. Colourless blocks of **1** were crystallised by vapour diffusion of Et_2O over 7 d and isolated in ~50% yield. Elemental analysis (%) calculated for $C_{14}H_{36}N_6O_{20}Gd_2$: C 18.22, H 3.93, N 9.11; found: C 18.28, H 3.67, N 8.66. Crystal data for **1**: $C_{14}H_{36}Gd_2N_6O_{20}$, M = 922.99, triclinic, a = 8.2904(3), b = 8.6272(3), c = 10.2877(3) Å, α = 86.684(3), β = 79.434(3), γ = 84.336(3)°, V = 719.20(4) Å^3, T = 100 K, space group $P\bar{1}$ (no. 2), Z = 1, reflections measured 11 286, 2823 unique (R_{int} = 0.0421) which were used in all calculations. The final R_1 was 0.0343 [for 2669 reflections with $I > 2\sigma(I)$] and the final w$R(F_2)$ was 0.0889 (all data). CCDC 1520393.†

$[Gd_2(H_2tea)(Htea)(NO_3)_3]_2{\cdot}MeOH$ (2·MeOH)

Triethanolamine (0.5 cm^3, 1.0 M solution in MeOH, 0.5 mmol) and $[NEt_4][OAc]{\cdot}4H_2O$ (0.131 g, 0.5 mmol) were added to a solution of $Gd(NO_3)_3{\cdot}6H_2O$ (0.226 g, 0.5 mmol) in MeOH (25 cm^3). NEt_3 (0.10 cm^3, 0.75 mmol) was added and the solution stirred for 1 h. Colourless prisms of **2** were crystallised by vapour diffusion of Et_2O over 14 d and isolated in 20% yield. Elemental analysis (%) calculated for $Gd_4C_{26}H_{62}N_{10}O_{32}$: C 18.85, H 3.77, N 8.46; found: C 18.48, H 3.78, N 8.21. Crystal data for **2**: $C_{26}H_{62}Gd_4N_{10}O_{32}$, M = 1655.86, monoclinic, a = 14.0518(4), b = 11.2346(3), c = 16.6847(5) Å, β = 103.776(3)°, V = 2558.18(13) Å^3, T = 100 K, space group $P2_1/c$ (no. 14), Z = 2, reflections measured 23 816, 5041 unique (R_{int} = 0.0853) which were used in all calculations. The final R_1 was 0.0752 [for 4333 reflections with $I > 2\sigma(I)$] and the final w$R(F_2)$ was 0.1991 (all data). CCDC 1520394.†

$[Gd(Htea)(NO_3)]_6{\cdot}8MeOH$ (3·8MeOH)

3 was prepared in a slight adaptation of the procedure described by Murray *et al.*[9f] Triethanolamine (0.5 cm^3, 1.0 M solution in MeOH, 0.5 mmol) was added to a solution of $Gd(NO_3)_3{\cdot}6H_2O$ (0.226 g, 0.5 mmol) in MeOH/CH_2Cl_2 (1 : 1 v/v) (25 cm^3). NEt_3 (0.14 cm^3, 1.0 mmol) was added and the solution stirred for 10 min. A white precipitate was removed by filtration and colourless plates of **3** were crystallised by slow evaporation over 2 d and isolated in 35% yield. Alternatively, **3** was also prepared by solvothermal methods by sealing $Gd(NO_3)_3{\cdot}6H_2O$ (0.226 g, 0.5 mmol), triethanolamine (0.5 cm^3, 1.0 M solution in MeOH, 0.5 mmol), NEt_3 (0.14 cm^3, 1.0 mmol) and MeOH (8 cm^3) in a Teflon lined bomb and heating to 130 °C for 24 h. After slow cooling **3** was isolated as large colourless crystals in ~60% yield. **3** can also be prepared without the addition of NEt_3, but the yield drops to approximately 30%. Elemental analysis (%) calculated for $Gd_6C_{44}H_{110}N_{12}O_{44}$: C 21.53, H 4.52, N 6.85; found: C 21.18, H 4.12, N 6.66. CCDC 751870.†

Acknowledgements

EKB thanks the EPSRC for funding. SGC, GL, ER and ME thank the Spanish Ministry of Economy, Industry and Competitiveness (MAT2015-68204-R and CTQ2015-64579-C3-1-P) and for a postdoctoral grant (to GL). ER acknowledges the Generalitat de Catalunya for an ICREA Academia grant and the BSC (Barcelona Supercomputer Center) for computational resources. KSM thanks the Australian Research Council for a Discovery grant.

Notes and references

1 (*a*) L. Engelhardt, M. Luban and C. Schröder, *Phys. Rev. B: Condens. Matter*, 2006, **74**, 054413; (*b*) A. Ghirri, A. Candini, M. Evangelisti, M. Affronte, S. Carretta, P. Santini, G. Amoretti, R. S. G. Davies, G. Timco and R. E. P. Winpenny, *Phys. Rev. B: Condens. Matter*, 2007, **76**, 214405; (*c*) A. Machens, N. P. Konstantinidis, O. Waldmann, I. Schneider and S. Eggert, *Phys. Rev. B: Condens. Matter*, 2013, **87**, 144409; (*d*) F. Adelnia, A. Chiesa, S. Bordignon, S. Carretta, A. Ghirri, A. Candini, C. Cervetti, M. Evangelisti, M. Affronte, I. Sheikin, R. Winpenny, G. Timco, F. Borsa and A. Lascialfari, *J. Chem. Phys.*, 2016, **143**, 244321.

2 NanoScience and Technology, in *Molecular Magnets: Physics and Applications*, ed. J. Bartolomé, F. Luis and J. F. Fernández, Springer-Verlag, Berlin, Heidelberg, 2014.

3 F. Luis and M. Evangelisti, *Struct. Bonding*, 2015, **164**, 431.

4 (*a*) K. A. Gschneidner Jr. and V. K. Pecharsky, *Annu. Rev. Mater. Sci.*, 2000, **30**, 387; (*b*) M. Evangelisti and E. K. Brechin, *Dalton Trans.*, 2010, **39**, 4672; (*c*) J. W. Sharples and D. Collison, *Polyhedron*, 2013, **54**, 91.

5 (*a*) P. Debye, *Ann. Phys.*, 1926, **386**, 1154; (*b*) W. F. Giauque, *J. Am. Chem. Soc.*, 1927, **49**, 1864.

6 (*a*) G. Lorusso, J. W. Sharples, E. Palacios, O. Roubeau, E. K. Brechin, R. Sessoli, A. Rossin, F. Tuna, E. J. L. McInnes, D. Collison and M. Evangelisti, *Adv. Mater.*, 2013, **25**, 4653; (*b*) M.-J. Martínez-Pérez, O. Montero, M. Evangelisti, F. Luis, J. Sesé, S. Cardona-Serra and E. Coronado, *Adv. Mater.*, 2012, **24**, 4301.

7 See, *e.g.*: (*a*) A. Benelli, C. Benelli, A. Caneschi, R. Carlin, A. Dei and D. Gatteschi, *J. Am. Chem. Soc.*, 1985, **107**, 8128; (*b*) M. Andruh, I. Ramade, E. Codjovi, O. Guillou, O. Kahn and J. C. Trombe, *J. Am. Chem. Soc.*, 1993, **115**, 1823; (*c*) J. P. Costes, F. Dahan, A. Dupuis and J. P. Laurent, *Inorg. Chem.*, 1997, **36**, 3429; (*d*) A. J. Blake, R. O. Gould, C. M. Grant, P. E. Y. Milne, S. Parsons and R. E. P. Winpenny, *J. Chem. Soc., Dalton Trans.*, 1997, 485; (*e*) C. Benelli and D. Gatteschi, *Chem. Rev.*, 2002, **102**, 2369; (*f*) M. Evangelisti, M. L. Khan, J. Bartolomé, L. J. de Jongh, C. Meyers, J. Leandri, Y. Leroyer and C. Mathonière, *Phys. Rev. B: Condens. Matter*, 2003, **68**, 184405; (*g*) B. W. Wang, S. D. Jiang, X. T. Wang and S. Gao, *Sci. China Ser. B: Chem.*, 2009, **52**, 1739.

8 (*a*) R. H. Laye and E. J. L. McInnes, *Eur. J. Inorg. Chem.*, 2004, 2811; (*b*) R. Shaw, R. H. Laye, L. F. Jones, D. M. Low, C. Talbot-Eeckelaers, Q. Wei, C. J. Milios, S. Teat, M. Helliwell, J. Raftery, M. Evangelisti, M. Affronte, D. Collison, E. K. Brechin and E. J. L. McInnes, *Inorg. Chem.*, 2007, **46**, 4968.

9 See for example: (*a*) N. F. Chilton, S. K. Langley, B. Moubaraki and K. S. Murray, *Dalton Trans.*, 2010, **46**, 7787; (*b*) S. K. Langley, N. F. Chilton, M. Massi, K. J. Berry and K. S. Murray, *Dalton Trans.*, 2010, **39**, 7236; (*c*) S. K. Langley, B. Moubaraki and K. S. Murray, *Dalton Trans.*, 2010, **39**, 5066; (*d*) S. K. Langley, B. Moubaraki, K. J. Berry and K. S. Murray, *Dalton Trans.*, 2010, **39**, 4848; (*e*) S. K. Langley, K. J. Berry, B. Moubaraki and K. S. Murray, *Dalton Trans.*, 2009, 973; (*f*) S. K. Langley, B. Moubaraki, C. M. Forsyth, I. A. Gass and K. S. Murray, *Dalton Trans.*, 2010, **39**, 1705; (*g*) T. C. Stamatatos, D. Foguet-Albiol, W. Wernsdorfer, K. A. Abboud and G. Christou, *Chem. Commun.*, 2011, **47**, 274.

10 S. K. Langley, N. F. Chilton, B. Moubaraki, T. Hooper, E. K. Brechin, M. Evangelisti and K. S. Murray, *Chem. Sci.*, 2011, **2**, 1166.

11 W. Plass and G. Fries, *Z. Anorg. Allg. Chem.*, 1997, **623**, 1205.

12 K. Manseki, H. Sakiyama, M. Sakamoto, Y. Nishida, H. Aono, Y. Sadaoka, M. Ohba and H. Okawa, *Synth. React. Inorg. Met.-Org. Chem.*, 2001, **31**, 1443.

13 S. Mathur, H. Shen, N. Lecerf, A. Kjekshus, H. Fjellvag and G. F. Goya, *Adv. Mater.*, 2002, **14**, 1405.

14 N. G. Naumov, M. S. Tarasenko, A. V. Virovets, Y. Kim, S. J. Kim and V. E. Fedorov, *Eur. J. Inorg. Chem.*, 2006, 298.

15 S. D. Daniel, J. S. M. Lehn, P. van der Heide, Y. Q. Wang and D. M. Hoffman, *Inorg. Chim. Acta*, 2006, **359**, 257.

16 L. Canadillas-Delgado, O. Fabelo, J. Pasan, F. S. Delgado, F. Lloret, M. Julve and C. Ruiz-Perez, *Dalton Trans.*, 2010, **39**, 7286.

17 Y. N. Guo, G. F. Xu, P. Gamez, L. Zhao, S. Y. Lin, R. P. Deng, J. K. Tang and H. J. Zhang, *J. Am. Chem. Soc.*, 2010, **132**, 8538.

18 H. S. Ke, G. F. Xu, Y. N. Guo, P. Gamez, C. M. Beavers, S. J. Teat and J. K. Tang, *Chem. Commun.*, 2010, **46**, 6057.

19 J. J. Borrás-Almenar, J. M. Clemente-Juan, E. Coronado and B. S. Tsukerblat, *J. Comput. Chem.*, 2001, **22**, 985.

20 (*a*) M. S. José, A. Emilio, D. G. Julian, G. Alberto, J. Javier, O. Pablo and S.-P. Daniel, *J. Phys.: Condens. Matter*, 2002, **14**, 2745; (*b*) E. Artacho, E. Anglada, O. Diéguez, J. D. Gale, A. García, J. Junquera, R. M. Martin, P. Ordejón, J. M. Pruneda, D. Sánchez-Portal and J. M. Soler, *J. Phys.: Condens. Matter*, 2008, **20**, 064208; L. Kleinman and D. M. Bylander, *Phys. Rev. Lett.*, 1982, **48**, 1425.

21 J. P. Perdew, K. Burke and M. Ernzerhof, *Phys. Rev. Lett.*, 1996, **77**, 3865.
22 V. Blum, R. Gehrke, F. Hanke, P. Havu, V. Havu, X. Ren, K. Reuter and M. Scheffler, *Comput. Phys. Commun.*, 2009, **180**, 2175.
23 A. D. Becke, *J. Chem. Phys.*, 1993, **98**, 5648.
24 (*a*) E. Cremades, S. Gómez-Coca, D. Aravena, S. Alvarez and E. Ruiz, *J. Am. Chem. Soc.*, 2012, **134**, 10532; (*b*) D. Aravena, D. Venegas-Yazigi and E. Ruiz, *Sci. Rep.*, 2016, **6**, 23847.
25 (*a*) M. E. Fisher, *Am. J. Phys.*, 1964, **32**, 343; J. H. Luscombe, M. Luban and F. Borsa, *J. Chem. Phys.*, 1998, **108**, 7266.
26 M. Evangelisti, O. Roubeau, E. Palacios, A. Camón, T. N. Hooper, E. K. Brechin and J. J. Alonso, *Angew. Chem., Int. Ed.*, 2011, **50**, 6606.